RSC Advances

PAPER

View Article Online
View Journal | View Issue

Cite this: *RSC Adv.*, 2026, **16**, 8322

Preparation of a new BTEAB/DMSO deep eutectic solvent for highly efficient starch dissolution and succinylation

Mohamed El Farkhani, *[ab] Omar Azougagh,[a] Mohamed Azzouzi, [ac] Said Dadou,[ab] Meryem Abida,[a] Mohamed El Miz,[a] Soufian El Barkany,[a] Noureddine Benchat[b] and Mohammed Koudad[a]

In this work, a novel deep eutectic solvents (DES) based on benzyltriethylammonium bromide/dimethyl sulfoxide (BTEAB/DMSO) is prepared and described. Comprehensive physicochemical analyses revealed a eutectic point at 0 °C, demonstrating the formation of a highly stable liquid phase characterized by strong intermolecular interactions between the two components. Beyond its original preparation, this DES proved to be an exceptionally efficient medium for biomass processing. It enabled the dissolution of up to 22 wt% of starch at 90–95 °C, a value significantly higher than typically achieved with other solvents. Moreover, the BTEAB/DMSO system served as a reactive medium, enabling direct esterification of starch with succinic anhydride under catalyst-free conditions, thereby simplifying the process and making it more environmentally sustainable. A full suite of structural, morphological, and thermal characterizations, including FTIR-ATR, H^1 NMR, XRD, SEM, EDX, and TGA, confirmed substantial modification of starch after treatment. The regenerated material exhibited a marked loss of crystallinity, the disappearance of native granules, changes in elemental composition, and a decrease in thermal stability, all of which are consistent with successful incorporation of succinyl groups. These results clearly demonstrate that the BTEAB/DMSO DES is not only a powerful solvent but also an effective reaction platform for starch valorization. Overall, this study introduces a highly promising, eco-friendly strategy for polysaccharide processing and opens new avenues for sustainable chemical transformations based on DES.

Received 20th November 2025
Accepted 28th January 2026

DOI: 10.1039/d5ra08988c

rsc.li/rsc-advances

1 Introduction

Starch is the second-most-abundant renewable raw material in nature, after cellulose. This natural polymer is readily available, biocompatible, and cost-effective.[1] Native starch is a semi-crystalline polymer consisting primarily of two types of α-glucans, linear amylose and highly branched amylopectin.[2] It contains numerous hydroxyl groups, allowing it to form both intramolecular and intermolecular hydrogen bonds.[3] It can thus form complex hydrogen-bonded networks, as well as regular and ordered crystalline arrangements among the polysaccharide chains of starch. These structural features result in the low solubility of starch in most conventional organic solvents,[4] restricting its modification and limiting its industrial applications. Although starch can dissolve in certain solvents, such as dimethyl sulfoxide (DMSO)[5–7] and dimethylacetamide/LiCl,[8,9] these solvents are not generally accepted in the industrial sector. As alternatives, ionic liquids (IL), including 1-allyl-3-methylimidazolium chloride, 1-ethyl-3-methylimidazolium acetate, and 1-butyl-3-methylimidazolium chloride, have been widely explored as promising "green solvents" to dissolve starch,[10] along with alkaline aqueous solutions (NaOH)[11] that usually require high temperatures or other specific operational conditions.[9]

Innovative and environmentally friendly solvents, such as deep eutectic solvents (DES),[12,13] have been investigated for their potential to dissolve starch and facilitate the development of starch-based materials.[14] DES are a novel class of IL analogs composed of hydrogen-bond acceptors and donors.[15] Eutectic mixtures are characterized by a low melting point, *i.e.*, they solidify or melt at temperatures lower than those of any of their individual components. This unique behavior arises from synergistic interactions between the constituent compounds, which disrupt the regular lattice structure and facilitate phase transitions at reduced temperatures.[16] They not only exhibit reaction properties similar to those of IL but also offer important advantages, such as low cost, high atomic utilization,

[a]*Laboratory of Molecular Chemistry, Materials and Environment (LMCME). Department of Chemistry, Faculty of Multidisciplinary Nador. Mohammed 1st University, PB300, Nador 62700, Morocco. E-mail: Mohamed.elfarkhani@ump.ac.ma*
[b]*Laboratory Applied Chemistry and Environmental (LCAE), Faculty of Sciences of Oujda. Mohammed 1st University, 60000 Oujda, Morocco*
[c]*Superior School of Technology of Khenifra (EST-Khenifra), University of Sultan Moulay Slimane, BP 170, Khenifra 54000, Morocco*

straightforward preparation,[17] and non-volatility.[18] Dingyi Shi *et al.* explored the viscosity of DES, a key physicochemical property that critically affects their practical applications in mass and heat transfer processes. As experimental viscosity determination is resource-intensive and influenced by operational factors, such as temperature and water content, the authors compiled a comprehensive dataset of viscosity measurements for 107 DES. They employed machine learning models to predict viscosity with high accuracy.[19] Consequently, DES have been recognized as promising alternative green solvents for polysaccharides, including starches,[20] lignin,[21] cellulose,[22] and even biomass.[23] The study showed that the most effective dissolution of starch was achieved using a mixture of choline chloride and urea 9.1 wt% and choline chloride and citric acid 8.3 wt% after heating at 100 °C. Additionally, 1-butyl-3-methylimidazolium chloride enabled solubility levels of up to 15 wt% at 80 °C. Comparable results were observed for potato starch dissolved in choline chloride/urea, choline chloride/citric acid, and choline chloride/succinic acid solutions after 60 min at temperatures between 118 and 135 °C.[9,24] In some studies, DES based on DMSO and choline chloride were prepared by heating an equimolar (1 : 1) mixture at 130 °C, leading to the formation of a homogeneous, transparent liquid within ~1 h. This behavior is attributed to strong hydrogen-bond interactions between choline chloride and DMSO, which markedly lower the melting point and yield a stable DES suitable as a green reaction medium.[25]

In this study, a novel DES was prepared by combining DMSO, an HBD, with benzyltriethylammonium bromide (BTEAB), an HBA. The system exhibited a melting point of 0 °C at molar fractions of 0.71 and 0.29 for DMSO and BTEAB, respectively. The dissolution and chemical modification capabilities of this system toward starch were investigated. Solubility measurements as a function of mass fraction revealed, for the first time to our knowledge, a starch solubility of 22% in a BTEAB/DMSO-based DES. This solvent proved particularly efficient for succinic anhydride esterification, operating without the need for conventional catalysts or organic solvents. X-ray diffraction analysis showed a marked decrease in the crystallinity index, which is consistent with the development of an amorphous structure upon dissolution. FTIR-ATR spectra showed no significant alteration in the major structural features, while thermogravimetric analysis (TGA) indicated a decrease in the degradation temperature. Scanning electron microscopy (SEM) images revealed the disappearance of starch granules, and energy dispersive X-ray spectroscopy confirmed the stability of the C/O atomic ratio before and after dissolution. Successful starch modification was further validated through FTIR-ATR and ^{1}H NMR analyses. Complementary characterizations, including SEM, EDX, and TGA, highlighted morphological, compositional, and thermal transformations.

To the best of our knowledge, the BTEAB/DMSO system has not been reported in the literature as a DES; its preparation, characterization, or practical applications have not been explored previously, underscoring the originality of this work. This paper is part of a comprehensive study, soon to be published, dedicated to an in-depth investigation of the BTEAB/DMSO system and its capacity to dissolve other biopolymers, and proposes a new strategy to lower the eutectic point (T_{eu}) from 0 °C to −10 °C.

2 Materials and methods

2.1. Materials

Potato starch (Sigma-Aldrich, CAS No. 9005-25-8, purity ≥99%; molecular weight and the content of amylose and amylopectin are unspecified and do not influence the results), succinic anhydride (Sigma-Aldrich, CAS No. 108-30-5, purity ≥99%), DMSO (Sigma-Aldrich, CAS No. 67-68-5, purity ≥99%), triethylamine (Sigma-Aldrich, CAS No. 121-44-8, purity ≥99%), benzyl bromide (Sigma-Aldrich, CAS No. 100-39-0, purity ≥99%), solvents (including tetrahydrofuran (Merck, CAS No. 109-99-9, purity ≥99%), diethyl ether (Merck, CAS No. 60-29-7, purity ≥99%), and ethanol (Merck, CAS No. 64-17-5, purity ≥99%)) were used without further purification after purchase to ensure experimental consistency.

2.2. Methods

2.2.1. Instrumental analysis. The chemical structures of the starch and S-MA samples were characterized by FTIR-ATR spectroscopy using a JASCO FT/IR-4700 spectrometer equipped with an ATR accessory. For each sample, an average of 70 scans was recorded over the spectral range of 4000 to 400 cm^{-1}. NMR spectra for both ^{1}H and ^{13}C were recorded using a JNM-ECZ500R/S1 FT NMR system (JEOL) operating at 500 MHz for ^{1}H and 126 MHz for ^{13}C. Chemical shifts are reported in parts per million (ppm) relative to the residual solvent peak and were determined using an internal reference. X-ray diffraction (XRD) patterns were acquired with a Bruker D8 Advance powder diffractometer (Germany) using Cu Kα radiation ($\lambda = 1.5418$ Å) at 40 kV and 40 mA. Scans were acquired within the 4–50° (2θ) range with a step size of 0.02° (2θ) and a scan rate of 0.02° (2θ) every 2 seconds. Surface morphology was investigated by scanning electron microscopy (SEM) on a Hitachi S-4800 instrument operated at 10 kV. The thermal stability of starch and S-SA samples was evaluated by thermogravimetric analysis (TGA) using the DTA PT 1600 instrument; scans were performed from ambient temperature to 570 °C at a heating rate of 10 °C min^{-1} under a nitrogen atmosphere, with alumina (Al_2O_3) crucibles serving as references.

2.2.2. Preparation of BTEAB. BTEAB was prepared following the procedure described by Azougagh *et al.*, as reported in our previous publication.[26] Briefly, benzyl bromide (4.5 ml. 38 mmol) was reacted with an equimolar amount of triethylamine (5 ml. 36 mmol) in tetrahydrofuran at room temperature. The white crystalline BTEAB salt obtained was separated by vacuum filtration, washed several times with diethyl ether, and dried under vacuum in a desiccator until a constant mass was achieved (Fig. 1). After this process, the yield was determined to be 94%.

2.2.3. Preparation of BTEAB/DMSO (1 : 2.5) deep eutectic solvent. The DES with a BTEAB/DMSO (1 : 2.5) composition was prepared by mixing 1 g of BTEAB (36.76 mmol) with 0.66 mL of

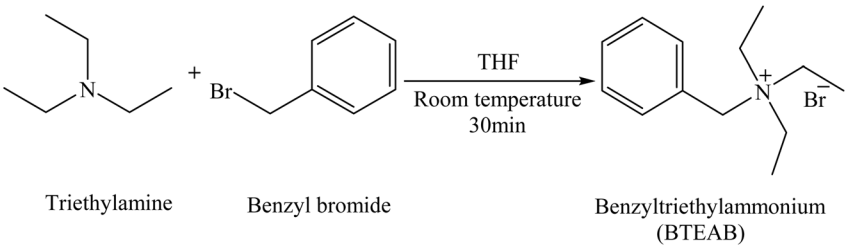

Fig. 1 Reaction scheme for the preparation of BTEAB.

DMSO (91.9 mmol). Continuous stirring of the mixture at 90–95 °C led to the formation of a homogeneous liquid phase, characteristic of DES formation.

2.2.4. Starch solubility in BTEAB/DMSO. To evaluate the solubility of starch in the BTEAB/DMSO DES, several solutions with starch concentrations of 10%, 20%, 22%, and 24% were prepared. For each concentration, a precise mass of starch was weighed and then gradually incorporated into the DES, which had been prepared beforehand and maintained at 90 °C under continuous stirring. The mixture was then stirred for 30 min until complete dissolution was achieved or until an insoluble residue was observed. Solubility was first assessed visually. It was then confirmed by precipitation in ethanol, followed by filtration. This protocol enables the determination of the maximum concentration of starch that can be dissolved in the BTEAB/DMSO DES.

2.2.5. Synthesis of S-SA esters. A total of 0.5 g of starch, which is equivalent to 0.0031 mol of anhydroglucose units (AGU), was incorporated into the DES. The mixture was heated at reflux at 90–95 °C until a uniform, viscous solution was obtained. Then, 1.24 g of succinic anhydride (0.0124 mol) was added without a catalyst, and the system was stirred at the same temperature for 4 h. The product thus obtained, *i.e.*, starch modified with succinic anhydride (S-SA), was isolated by precipitation in ethanol, then filtered under vacuum and purified with ethanol in a soxhlet extractor for 48 h to remove residual traces of DES and unreacted anhydride. After drying in a desiccator containing P_2O_5 for one week, a constant weight was achieved. The eutectic solvent was regenerated by removing impurities and residual solvents by evaporation under reduced pressure.

2.2.6. Determination of DS. The degree of substitution in the S-SA sample was quantified from its respective ^{1}H NMR spectra using eqn (1). This method, previously established in the literature,[27] enables an accurate estimation of the extent of succinyl groups introduced into the starch backbone by comparing the integrated proton signals of substituted and native structural units.

$$\mathrm{DS} = \frac{\text{area of H} - 7,8 \text{ proton of succinylated part}/4}{\text{area of H} - 1 \text{ proton of starch ackbone}} \quad (1)$$

3 Results and discussions

3.1. Preparation of DES

3.1.1. BTEAB/DMOS phase diagrams. A thermodynamic or a solid/liquid equilibrium diagram is a common method to define a binary eutectic system. It is a graph showing the molar ratio of one component and the melting events of the binary system. It is characterized by two lines: the solidus line, an almost horizontal line, representing the invariant low eutectic melting transition (regardless of molar composition) below which the system is in the solid state, and the liquidus line, which signifies the complete transition from the solid to the liquid state of the multicomponent system. These two lines are generated by varying the molar ratio of one component relative to the other and measuring the sequential thermal events for each composition using a differential scanning calorimetry trace. The liquidus line shows the variation in melting of the excess solid, with a distinct V-shape that is most often observed in binary eutectic mixtures,[28,29] as illustrated in Fig. 2a. The eutectic point is the intersection of the solidus and liquidus lines and corresponds to the molar composition at which the system reaches its minimum melting temperature. In the binary DMSO/BTEAB system, increasing the molar fraction of either component led to a progressive decrease in the melting temperature until this point was reached, where both constituents melted simultaneously at a constant temperature, following a typical eutectic diagram with a linear solidus line and a V-shaped liquidus line.[30,31] In conclusion, we have determined that the eutectic point of the BTEAB/DMSO mixture is 0 °C. This system allows a significant reduction in the melting temperatures of the pure components: 194 °C for BTEAB and 19 °C for DMSO. To the best of our knowledge, this DES based on the BTEAB/DMSO pair is reported here for the first time.

3.1.2. FTIR analysis. In this study, FTIR-ATR spectroscopy was employed to examine the DES obtained by mixing pure BTEAB with pure DMSO. Fig. 3 presents the FTIR-ATR spectra of BTEAB, DMSO, and the BTEAB/DMSO mixture.

For BTEAB, characteristic peaks corresponding to the quaternization of triethylamine are observed. New absorption bands appear, which are attributed to the out-of-plane bending of monosubstituted aromatic C–H bonds at 750 cm^{-1} and the angular deformation of aromatic C=C bonds at 704 cm^{-1},[32,33] indicating the incorporation of benzyl groups into the TEA structure. Another band at 1476 cm^{-1} is characteristic of the ethyl groups of the quaternary ammonium moiety.[34] The appearance of a strong peak at 2970 cm^{-1} in the spectrum is attributed to the stretching vibration of the methylene (–CH_2) group.[35–39] In the case of DMSO, the –CH_2– and –CH_3 groups exhibit characteristic stretching bands at 2918 cm^{-1} and 2970 cm^{-1}, respectively. Another band at 1016 cm^{-1} corresponds to the stretching vibration of the S=O group. The O–H

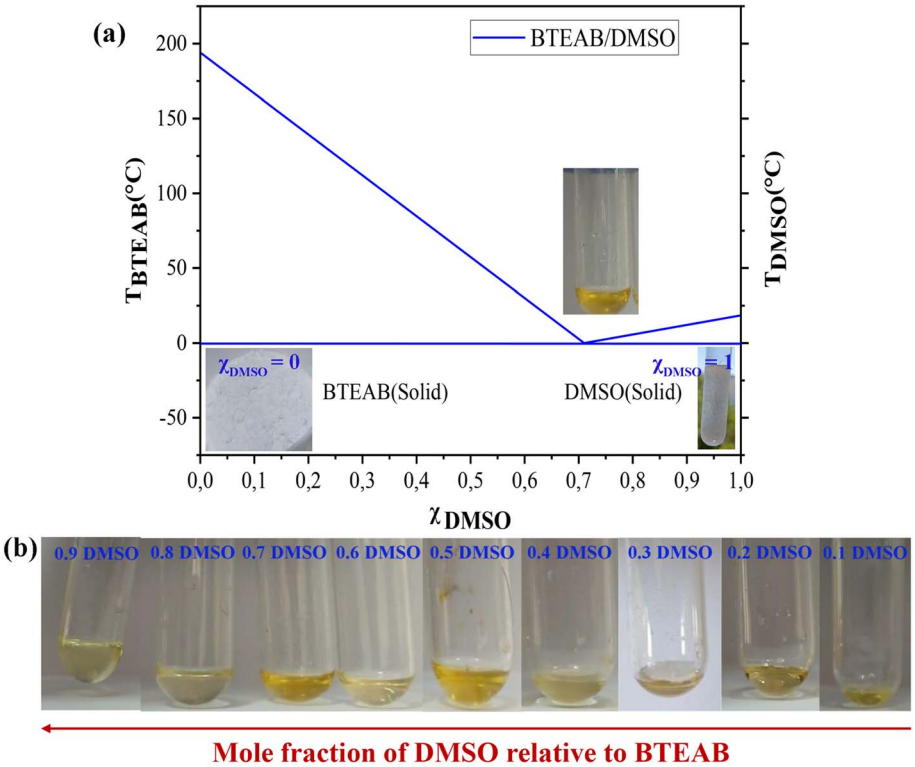

Fig. 2 (a) Phase diagrams of the binary eutectic system comprising BTEAB/DMSO, (b) photos of DES with different fractions of DMSO relative to BTEAB at different melting points.

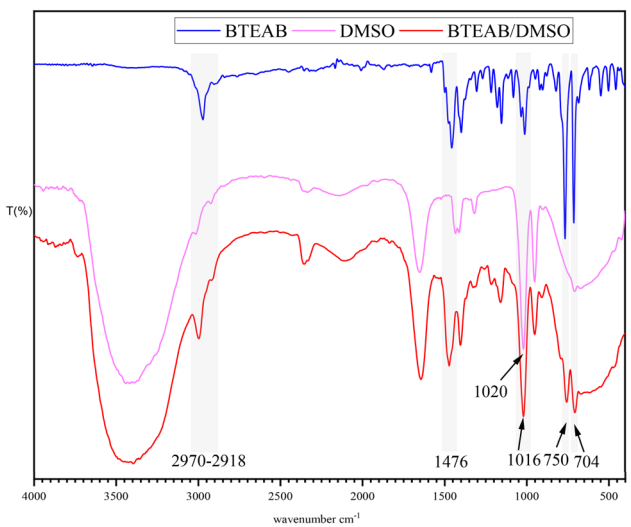

Fig. 3 FTIR-ATR spectra of BTEAB, DMSO, and BTEAB/DMSO.

band observed in the spectrum of the DMSO/BTEAB mixture is attributed to residual moisture present in both DMSO and the DES. In this mixture, the O–H band appears broadened, indicating enhanced and intensified hydrogen bonding within the system.[40] The infrared spectrum of the DES obtained from mixing DMSO with the quaternary ammonium salt BTEAB is shown in Fig. 3 with distinctive changes, highlighting molecular interactions between the two components. The emergence of new bands at 2973 cm^{-1} and in the 750–850 cm^{-1} region was assigned to C–H stretching of methyl groups and aromatic ring deformations, respectively, confirming the incorporation of BTEAB into the DES matrix.[41] Furthermore, the peak corresponding to the S=O group remains clearly visible in the DES spectrum, indicating the presence of DMSO. These spectral changes collectively demonstrate the formation of an extensive hydrogen bonding network between DMSO and salt ions, supporting both the formation and stability of the DES.[42]

3.2. Starch dissolution in the BTEAB/DMSO DES: experimental investigation

The starch solutions prepared in the BTEAB/DMSO mixture (1 : 2.5) exhibit macroscopic homogeneity, as illustrated in Fig. 4. However, a noticeable color change occurs at the highest starch concentrations. Table 1 presents the corresponding starch solubility percentages across the different systems investigated, providing a comparative overview of their dissolution behavior.

The solubilization results were obtained without starch pretreatment or the addition of additives to the BTEAB-based DES. It is reasonable to assume that DMSO, a hydrogen-bond donor, plays a key role in forming hydrogen bonds within the system. Its interaction with starch facilitates the breakdown of the hydrogen-bond network and stabilizes starch chains in the solvent, leading to a homogeneous solution and good starch solubility. DES (BTEAB/DMSO) showed effective solvation capacity across starch concentrations ranging from 10 to 22%, consistent with the literature. However, when the concentration

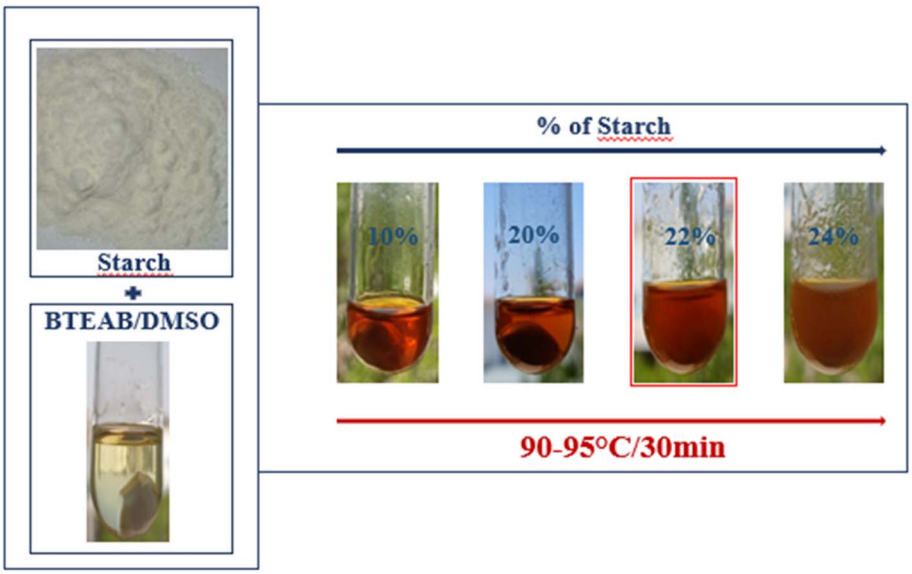

Fig. 4 Macroscopic observations of the BTEAB/DMSO and starch-BTEAB/DMSO mixture with 10, 20, 22, and 24 wt% of starch at 90–95 °C after 30 min.

exceeded 22%, solubility decreased to 24%, starch particles remained in suspension, and some of the swollen starch remained undissolved. These observations highlight the potential of the BTEAB/DMSO system at a 1 : 2.5 molar ratio as one of the most promising "green" DES, offering a sustainable, environmentally friendly alternative.

3.2.1. Effect of DES on the average molecular weight of starch. The determination of experimental viscosity is currently one of the most popular and oldest techniques in macromolecular chemistry for characterizing polymers in solution through their flow behavior.[45] In practice, the intrinsic viscosity method of a starch solution is often used to evaluate the average length of polysaccharide chains,[46] whose average molecular weight determined by viscometric techniques, notably using a Ubbelohde viscometer, can be defined as the viscosity-average molar mass, M_v. Intrinsic viscosity is directly related to the cohesive forces between macromolecular chains. Indeed, the density of supramolecular interactions increases with increasing macromolecular mass (as the chains become longer), and consequently, the cohesive forces become stronger, leading to increased resistance to flow.[45] To evaluate the stability of the macromolecular properties of starch in the BTEAB/DMSO system used as a DES, the structural changes of starch before and after dissolution were investigated. In this context, a Ubbelohde-type viscometer was used to determine the intrinsic viscosity (η_{int}) of starch in the KOH system by applying the Mark–Houwink equation (eqn (2)).

$$\eta_{int} = 1.18 \times 10^{-5} \times M^{0.89} \quad (2)$$

Viscosity measurements were carried out using a Ubbelohde capillary viscometer immersed in a water bath maintained at 25 °C. The concentrations of the studied commercial and regenerated starch solutions ranged from 0.1 to 0.5 g dL^{-1} and were prepared accordingly. Both starch samples were dissolved in a NaOH solution before the measurements. The capillary flow time of the polymer solutions was measured under identical conditions. Finally, the intrinsic viscosity was determined by extrapolating the inherent and reduced viscosities to zero concentration (Fig. 1S).[46] The M_w values calculated from intrinsic viscosity measurements for each starch sample, using the Mark–Houwink equation, were found to be 4.9×10^5 g mol^{-1} for the commercial starch and 4.5×10^5 g mol^{-1} for the regenerated starch. The BTEAB/DMSO solvent system does not apparently affect the polymer chain length of the starch sample after dissolution.

3.2.2. FTIR-ATR analysis. The impact of starch dissolution in the DES was evaluated by analyzing spectral changes in both

Table 1 Starch solubility in different systems

Solvents	Temperature (°C)	Solubility percentage	Ref
Choline chloride/urea	100	9.1% w/w	43
Choline chloride/citric acid	100	8.3% w/w	43
Choline chloride/succinic acid	118–135	—	43
Choline acetate	110	10%	44
Choline lactate	120	10%	44
BTEAB/DMSO	90–95	22%	This study

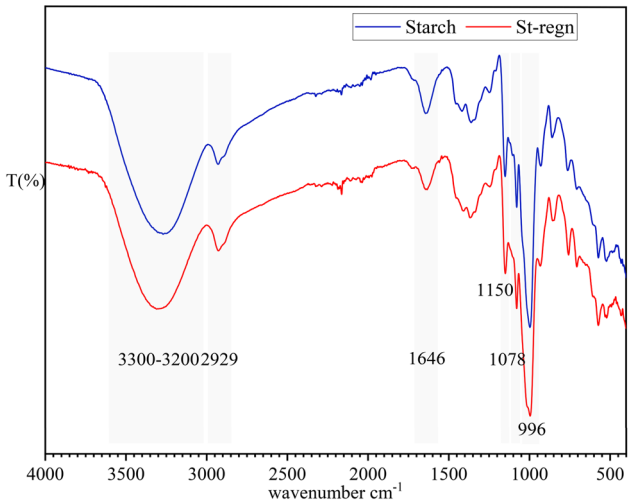

Fig. 5 FTIR-ATR of starch and regenerated starch (St-regn).

native and regenerated starch (Fig. 5). The characteristic absorption band at 3272 cm^{-1} corresponds to the O–H stretching vibration in starch.[47,48] Prominent peaks at 2930 cm^{-1} and 2892 cm^{-1} are linked to the stretching vibrations of methyl and methylene ($-CH_2$) groups. The signal at 1644 cm^{-1} is attributed to the adsorption of water in the amorphous regions of the starch structure. The bands at 1457 cm^{-1} are assigned to O–H bending in CH_2 groups.[35–39] The peak at 1644 cm^{-1} is attributed to water adsorption in the amorphous region of starch.[39] The bands at 1457 cm^{-1} are assigned to O–H bending in CH_2 groups.[49,50] In the region between 1300 and 1500 cm^{-1}, multiple overlapping bands are observed, corresponding to C–O–H bending, CH_2 twisting and bending, and C–O–C stretching vibrations.[51,52] weak band at 1244 cm^{-1} is associated with vibrations related to the CH_2OH side chain and C–O–H deformation modes.[53,54] The absorption peak around 1150 cm^{-1} is due to C–O stretching in the C–O–H group,[49,53,55] while the signal at 1077 cm^{-1} is attributed to C–O–C stretching vibrations. The band at 996 cm^{-1} corresponds to asymmetric skeletal vibrations within the starch ring structure.[49] Lower wavenumber absorptions include vibrations of the α-1,4 glycosidic bond at 923 cm^{-1} and C–H and CH_2 deformation modes at 861 cm^{-1}.[35] Finally, the absorption band at 761 cm^{-1} is ascribed to C–C stretching vibrations.[35,49] These findings indicate that the regenerated starch retains its native structural features, even after dissolution in the DES.

3.2.3. X-ray diffraction patterns analysis. Crystallinity is a central aspect of research on starch structure, encompassing the study of relative crystallinity and the determination of crystalline type, primarily *via* XRD.[56] In this study, the impact of the starch dissolution process in the DES BTEAB/urea was evaluated by analyzing the changes in the crystalline behavior and polymorphism of the regenerated starch. XRD was used to characterize the alterations in the long-range crystalline structures of native and regenerated starch. The corresponding diffractograms are presented in Fig. 6. Native starch shows several characteristic peaks located at $2\theta = 5.76°$, 15.26°, 17.32°, 19.92°, 22.30°, 24.22°, 26.32°, 30.96°, and 34.4°, indicating a B-type crystallinity.[57] The crystallinity index (X_c) was calculated following the procedure outlined by Cheetham *et al.*[58] using eqn (2) and (3), where H_c and H_a represent the intensities of the crystalline and amorphous peaks, respectively.

$$X_C = \frac{H_c}{H_c + H_a} \quad (3)$$

The crystallinity index of native starch reaches 80.75%. Amylose and amylopectin are the two main components of starch, with their contents being inversely proportional. The crystallinity of starch granules is primarily influenced by the crystalline regions of amylopectin.[59] The regenerated starch displays a reduced degree of crystallinity compared to the native starch, indicated by the loss of diffraction peaks at 2θ values of 5.76°, 15.26°, 17.32°, 19.92°, 22.30°, 24.22°, 26.32°, 30.96°, and 34.4°, alongside a broadening of the peak around 20.38°.[60] This modification results in the appearance of an amorphous peak, indicating a loss of crystalline order. This decrease in crystallinity is attributed to the action of the BTEAB/DMSO-based DES, which disrupts and destroys the native starch's original crystalline structure.

3.2.4. Scanning electron microscopy (SEM) – energy dispersive X-ray (EDX) analysis. SEM images of starch samples before and after solubilization in the BTEAB/DMSO system are shown in Fig. 7. Starches display a wide range of morphologies that vary according to their source and the synthesis methods employed. In synthetic starch, SEM images reveal granules with spherical, ellipsoidal, or oval shapes. Generally, smaller granules tend to be spherical, whereas larger ones often adopt an oval form, illustrating a pronounced heterogeneity in both size and shape. These observations are consistent with the average molecular weights determined for different starch types, as discussed in the next section. Moreover, various studies have demonstrated a relationship between granule morphology and the viscosity of starch solutions; higher viscosity typically promotes the formation of spherical droplets, which

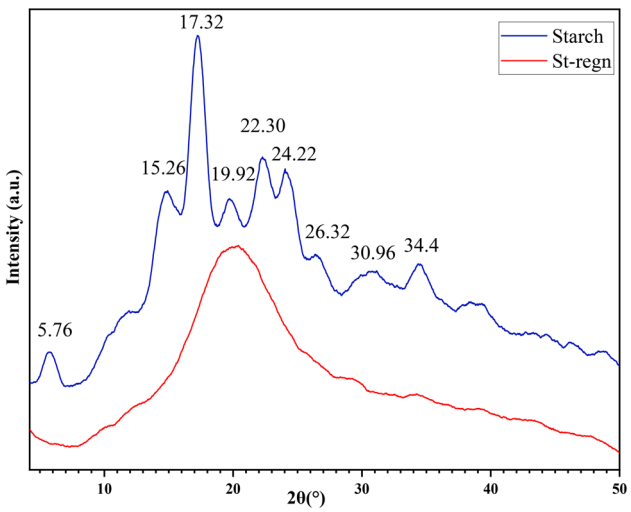

Fig. 6 XRD spectra of starch and regenerated starch (St-regn).

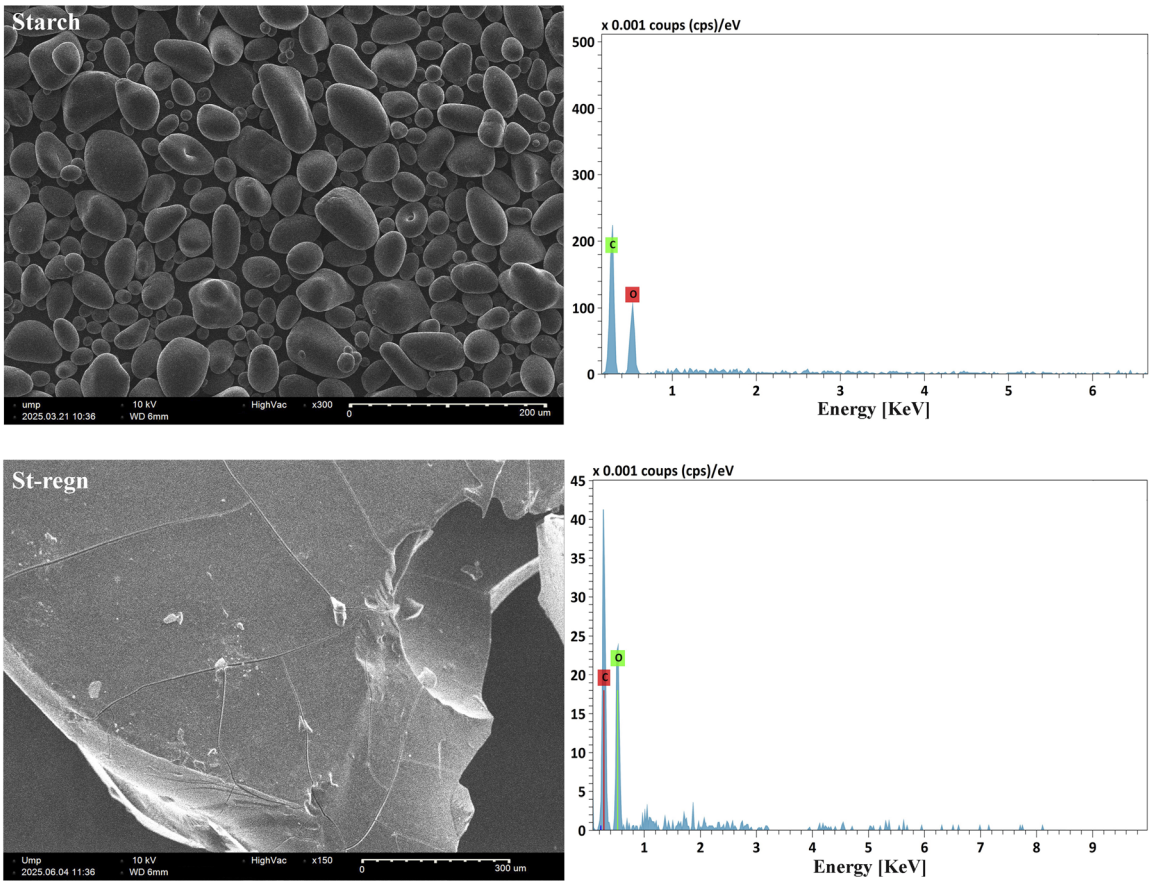

Fig. 7 SEM of starch and regenerated starch.

subsequently evolve into similarly shaped granules. The amylose-to-amylopectin ratio also plays a significant role in determining granule morphology, with higher amylose content leading to larger and more irregularly shaped granules.[61] After dissolution of starch in the BTEAB/urea system, the granules completely disappear, and noticeable cracks form within the structure. Treatment with the DES generates fine fissures and surface depressions, clearly indicating surface modification. The pronounced effect of DES on the granule structure is evident, as numerous cracks and streaks emerge following dissolution, highlighting significant morphological disruption. Conversely, when starch is only exposed to DES without complete dissolution, the granules undergo less severe degradation, showing only minor microcracks. Similar results have been observed with other starch types, reinforcing the conclusion that DES can partially disrupt granular structures.[62] The EDX spectra show a remarkable stabilization of the C/O ratio. In particular, this ratio is 2.003 for native starch and 1.966 for regenerated starch, indicating that the carbon content remains essentially unchanged after regeneration. This stability suggests that no significant chemical structural modifications occur during starch dissolution in the DES, highlighting the effectiveness and appropriateness of the experimental solubilization approach employed.

3.2.5. Thermal stability (TGA). TGA is an effective method for evaluating the thermal stability of diverse organic compounds, particularly carbohydrate-based polymers.[63] Gaining insight into the thermal degradation behavior and decomposition mechanisms is crucial for optimizing processing parameters. Analyzing the kinetics of the distinct decomposition phases can help elucidate the associated degradation routes. TGA is a dependable technique for assessing the thermal stability of various organic substances. As depicted in Fig. 8, thermal degradation for both native starch and St-regn counterpart occurred in two distinct stages. The TGA data revealed a lower degradation temperature for the St-regn than for the native starch.

The thermal behavior of starch after dissolution and regeneration in BTEAB/DMSO systems, as examined by TGA, reveals notable differences.[64] The thermograms (Fig. 8) display two main stages: an initial weight loss occurring between 60 °C and 90 °C, attributed to the removal of solvents and adsorbed moisture.[65] followed by a second stage at higher temperatures, corresponding to the degradation of the starch backbone. The peak degradation temperature shifts from 251.86 °C for native starch to 242.27 °C for the regenerated form. This reduction in the thermal degradation temperature is likely linked to the disruption of intra- and intermolecular interactions between

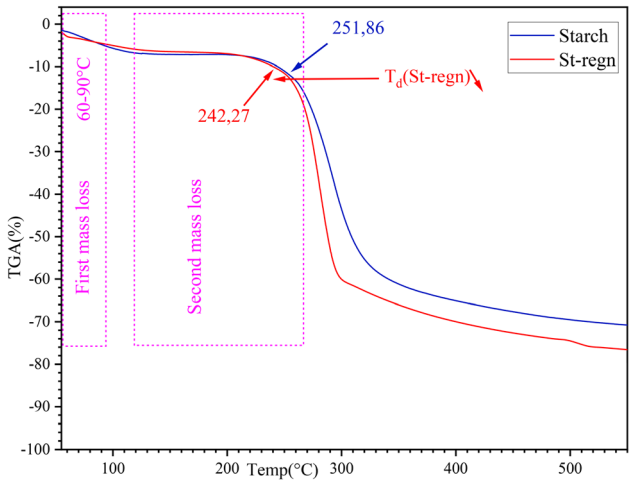

Fig. 8 TGA of starch and St-regn.

starch chains during dissolution,[66] as DES systems significantly disrupt hydrogen bonding, thereby reducing thermal stability.

3.3. Synthesis and application

In this study, the ion donor, BTEAB, was synthesized *via* a classic quaternization reaction between a tertiary amine (TEA) and an alkyl halide, benzyl bromide, in equimolar proportions. The reaction, carried out at room temperature in THF, gradually led to the formation of the quaternary salt BTEAB. Subsequently, a new BTEAB-based DES was developed by combining it for the first time with DMSO in a molar ratio of 1 : 2.5. Under stirring, the mixture showed a transition to the liquid state at a temperature between 90–95 °C. Further analysis determined that the eutectic point of this system is approximately 0 °C, reflecting the strong interaction between the components and confirming the formation of a truly thermodynamically stable DES. Finally, the starch esterification reaction shown in Fig. 9 was carried out in two distinct steps. First, the starch was completely dissolved in the BTEAB/DMSO mixture, demonstrating the solvating capacity of this new DES. Second, succinic anhydride was added to the reaction medium, enabling grafting onto the starch chain *via* esterification without an additional catalyst. This synthetic strategy illustrates the effectiveness of this DES system for the chemical modification of biopolymers under mild and environmentally friendly conditions.

DES plays a pivotal catalytic role in the esterification of biopolymers, such as starch, by functioning simultaneously as solvents and catalysts. By effectively disrupting the intra- and intermolecular hydrogen-bond network of the biopolymer, DES enhances the accessibility and reactivity of hydroxyl groups. The anions (Br^-) in the HBA component, particularly those with strong proton-accepting capabilities, facilitate the activation of –OH groups, while electrostatic interactions and hydrogen bonding with the esterifying agent promote polarization of the carbonyl group, thereby accelerating ester bond formation. Furthermore, the high polarity of DES stabilizes reaction intermediates and transition states, improving reaction kinetics and enabling higher degrees of substitution. Finally, the partial or complete dissolution of the biopolymer in DES creates a homogeneous reaction medium, ensuring uniform and efficient esterification under milder, environmentally benign conditions.[67] Fazal Haq *et al.* synthesized succinylated starches by reacting native starch with succinic anhydride and evaluated their adsorption potential for phenol, a toxic environmental pollutant. The modified starches exhibited significantly greater phenol uptake than unmodified starch, indicating that the introduction of carboxyl groups enhances interactions with phenol molecules. These findings suggest that succinylated starches are effective, biodegradable, and eco-friendly adsorbents to treat phenol-contaminated aqueous effluents.[68] Succinylated starches with DS ranging from 0.0123 to 0.0427 were synthesized by Feng Cao *et al.* The authors demonstrated that these modified starches exhibited a significant adsorption capacity for methylene blue, reaching 24.3962 mg g^{-1}, highlighting their potential as effective adsorbents in aqueous systems. These observations suggest that the introduction of succinyl groups enhances the interaction between the starch matrix and the dye molecules, thereby improving the overall adsorption efficiency.[69]

3.4. Spectral and structural analyses

3.4.1. Vibrational spectroscopy FTIR-ATR. The reaction of starch modification with succinic anhydride was analyzed by Fourier transform infrared spectroscopy. The appearance of new absorption bands that were characteristic of the introduced functional groups, particularly those associated with ester functions, was accompanied by a decrease or disappearance of certain bands specific to the initial functional groups of starch.

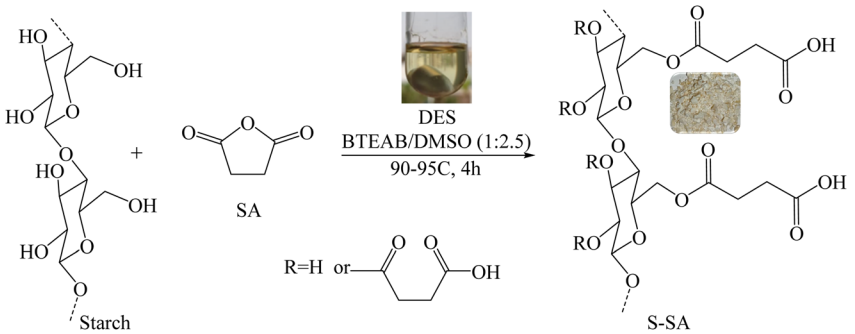

Fig. 9 Reaction scheme for the preparation of S-SA from starch in BTEAB/DMSO.

These trends indicate the effective progression of the esterification reaction. Spectroscopic analysis thus highlighted the formation of ester bonds between the hydroxyl groups of starch and the anhydride cycles of the reagent, confirming the success of the chemical modification (Fig. 10).

The absorption band observed at 3272 cm^{-1} in the starch spectrum corresponds to the O–H stretching vibration.[47,48] Two prominent peaks located at 2925 cm^{-1} are attributed to the stretching vibrations of methyl and methylene ($-CH_2$) groups.[35–39] The signal at 1644 cm^{-1} is linked to water adsorption within the amorphous regions of the starch structure.[39] The band at 1457 cm^{-1} is associated with the bending vibrations of the O–H groups in CH_2 moieties.[49,50] In the spectral region between 1300 and 1500 cm^{-1}, several overlapping bands are present, corresponding to C–O–H bending, CH_2 twisting and bending, and C–O–C stretching vibrations.[51,52] A weak band at 1244 cm^{-1} is attributed to the CH_2OH side-chain vibration, as well as to C–O–H deformation modes.[53,54] The absorption peak near 1150 cm^{-1} is assigned to the C–O stretching of the C–O–H group,[49,53,55] while the peak at 1077 cm^{-1} is associated with C–O–C stretching. The band at 996 cm^{-1} corresponds to skeletal vibrations of the asymmetric starch ring.[49] Low-wavenumber absorptions include the skeletal vibrational modes of the α-1,4-glycosidic bond at 923 cm^{-1} and the C–H and CH_2 deformation at 861 cm^{-1}.[35] Finally, the absorption band observed at 761 cm^{-1} is attributed to the C–C stretching vibration.[35,49]

In the FTIR spectrum of S-SA, the broad band around 3299 cm^{-1} shows a noticeable decrease in intensity. This reduction is likely due to fewer hydroxyl groups, resulting from their esterification with succinic anhydride.[70] Additionally, a new absorption band appears at 1730 cm^{-1} in the FTIR spectrum of S-SA, which is absent in the native starch spectrum. This band corresponds to the stretching vibration of the carbonyl (C=O) group, typical of ester and carboxylic acid functionalities, as illustrated in Fig. 10. Its presence provides further evidence of the esterification reaction between starch and succinic anhydride.[71] These observations confirm the successful progression of the esterification process. Moreover, a characteristic band at 1234 cm^{-1}, attributed to the stretching vibration of the ester O–C=O bond, is also detected. This is the result of the ring-opening of succinic anhydride, followed by its esterification with starch. Altogether, spectral data confirm the incorporation of succinic anhydride into the starch backbone, validating the formation of ester linkages between both components.[72]

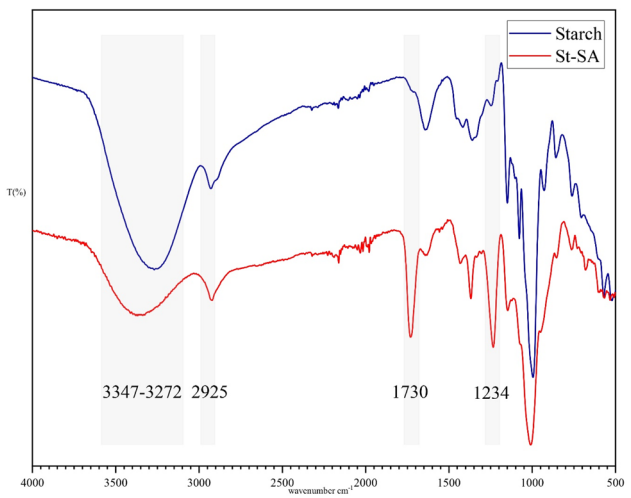

Fig. 10 FTIR-ATR spectra of starch and S-SA.

3.4.2 ^{1}H NMR spectra. Fig. 11a shows the ^{1}H NMR spectrum of the native starch sample. A prominent resonance at 3.15 ppm is assigned to residual water. The H-1 proton, on the glycosidic carbon, appears at δ ~4.2 ppm, reflecting its proximity to electronegative oxygen atoms. The hydroxyl protons, OH-2, OH-3, and OH-6, display distinct chemical shifts despite being bonded to oxygen, owing to differences in their immediate chemical environments. Notably, OH-6, which lies adjacent to a substituent with lower electron density, resonates at δ = 3.6 ppm, whereas OH-2 and OH-3 affected by similar neighboring groups and by the oxygen atoms involved in the glycosidic linkage are shifted downfield to δ = 5.08 ppm.[73,74] Signals at 3.64 ppm, 3.63 ppm, and 3.55 ppm correspond to the H-3, H-5, and H-6 protons of the anhydroglucose unit, respectively. Additionally, the peaks at 3.31 ppm and 3.33 ppm are attributed to the H-2 and H-4 protons of the AGU.[75]

Moreover, compared with native starch, the modified S-SA sample showed additional characteristic chemical signals: the CH_2 protons of the succinate group (H-7 and H-8) appeared at 2.45 and 2.55 ppm.[76] With respect to the proton shifts on the glucose residue, the signal observed at 5.06 ppm was attributed to the OH-2 and OH-3 proton environments in both starch and S-SA samples.[69] The appearance of additional signals at 4.17 and 4.31 ppm, corresponding to the H-6 and H-6′ protons, in the NMR spectra of S-SA confirms the successful esterification of starch by succinic anhydride, in line with the FT-IR observations. Moreover, the esterification process formed a covalent bond between succinic anhydride and the starch backbone.[77] The DS was then calculated using eqn (1), revealing a value of 0.82. This DS value reflects the average number of hydroxyl groups per anhydroglucose unit that were successfully replaced during the esterification process, providing a clear indication of the reaction's efficiency under the experimental conditions used.

The ^{13}C NMR spectrum of the S-SA confirms the successful grafting of the succinate group, with chemical shift variations observed for the C1 to C6 carbons of the AGU, as illustrated in Fig. 11b. In starch, the C6 carbon atoms bear primary hydroxyl groups that generally participate in intramolecular hydrogen bonding with the hydroxyl groups at C2, as well as in intermolecular hydrogen bonding with the C3 hydroxyls of the neighboring chains. Disruption of these hydrogen bonds, which is associated with a reduction in crystallinity, typically influences the resonance signals corresponding to the C6 carbons.[78] The C1 and C4 carbons of adjacent glucose units linked by the glycosidic bond C1–O–C4 do not engage in hydrogen bonding; therefore, they do not contribute to the crystallinity of starch. Consequently, the starch spectrum shows signals for the C6 carbon at 61.25 ppm, the C1 carbon at 100.7 ppm, and the C4 carbon at 79.5 ppm. Meanwhile, the overlapping signals of the

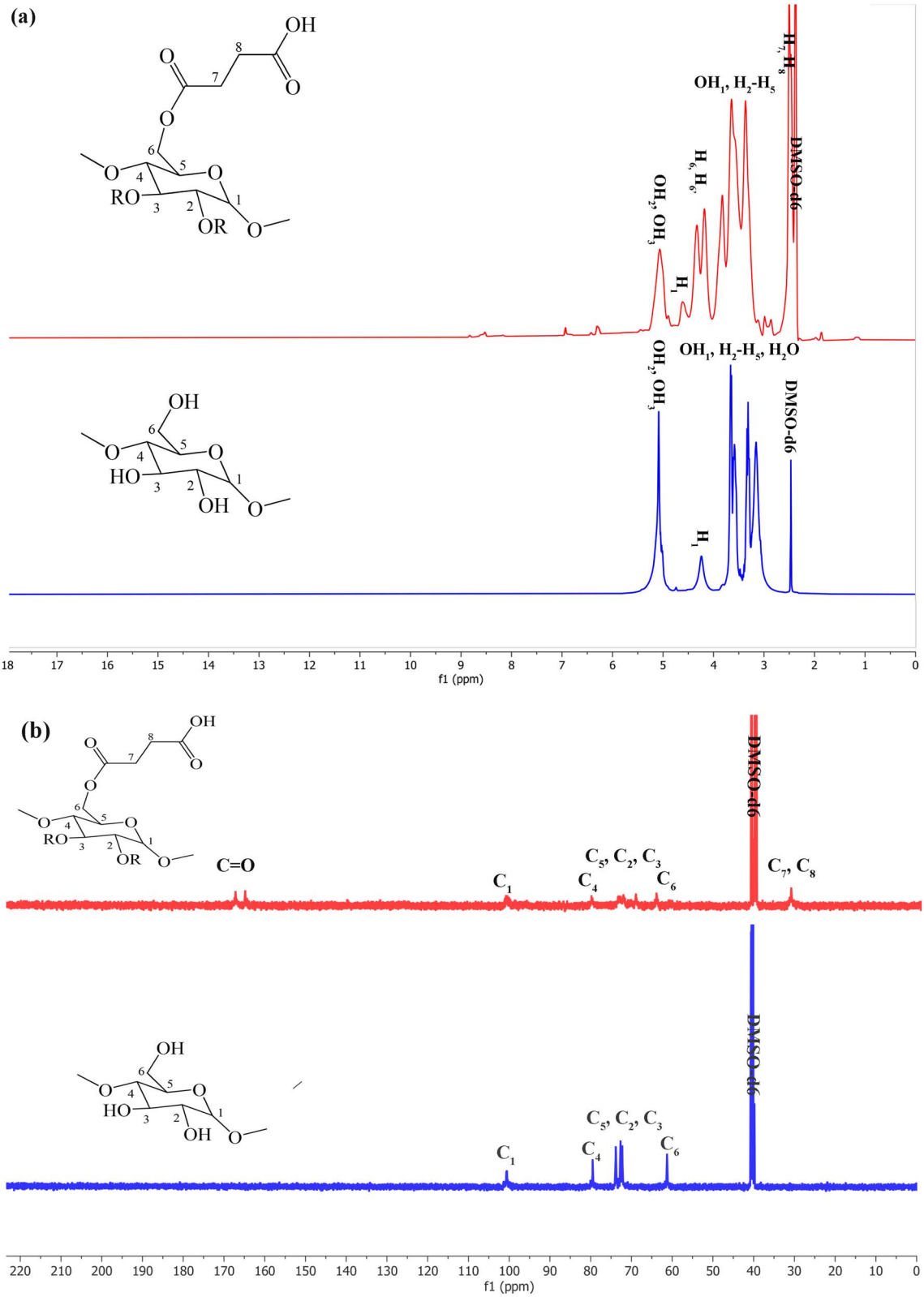

Fig. 11 (a) ^{1}H NMR spectra of starch and S-SA (b) ^{13}C NMR spectra of starch and S-SA.

C2, C3, and C5 carbons appear within the 71–74 ppm range.[79–83] Overall, the chemical shifts of the C1 and C4 carbons are particularly responsive to structural changes within each AGU, especially after the incorporation of succinic anhydride. Furthermore, minor changes in the C6 resonance can also impact the signals observed for the C1 and C4 carbons.[83,84] After

the esterification reaction, a singlet peak, corresponding to the C1 carbon of S-SA, was observed at 101 ppm. The decreased signal intensities of the C6 and C2,3, and 5 carbons provided evidence for the effective incorporation of the carboxylic acid groups onto the hydroxyl groups at C6, C2, and C3.[85] Significant signals were detected at 166.8 ppm and 165.7 ppm; they were attributed to the overlapping carbonyl resonances of the ester C═O and carboxylic acid COOH groups present in the S-SA segment. The peaks at 30.8 ppm were assigned to the unsaturated carbons C7–C8 within the succinate structure.[86]

3.4.3. Scanning electron microscopy (SEM) – energy dispersive X-ray (EDX) analysis. SEM is one of the most commonly used techniques for the textural analysis of materials, particularly to observe surface morphology. It offers nanometric resolution and a high depth-of-field, enabling detailed visualization of surface structures at different scales. In addition, EDX, often coupled with SEM, enables precise elemental analysis, thereby contributing to the local chemical characterization of samples.

As part of this study, the esterification of starch by succinic anhydride in a BTEAB/DMSO medium was confirmed by SEM imaging coupled with EDX analysis. Fig. 12 shows micrographs of the starch and esterified starch (S-SA) samples, highlighting the morphological changes induced by the chemical reaction. The associated EDX data identify the characteristic elements introduced during grafting, confirming the presence of functional groups derived from succinic anhydride on the surface of the modified starch. This dual SEM/EDX approach is therefore essential for visually and chemically corroborating the success of the functionalization. Starches exhibit a diverse granular morphology, reflecting heterogeneity in particle shape and size. Micrographs from an electron microscope reveal that synthetic starch granules adopt spherical, ellipsoidal, or oval shapes. Smaller granules are generally spherical, while larger ones tend to be oval. This morphological diversity can be attributed to the synthesis conditions and the intrinsic chemical composition of the starch.[87] These observations are consistent with the average molecular weight values that will be discussed in the following section. Furthermore, several studies have highlighted a correlation between the morphology of starch granules and the rheological properties of solutions. In particular, it has been shown that high viscosity promotes the formation of spherical droplets during gelatinization, thus leading to spherical-shaped granules. In addition, the composition of amylose and amylopectin plays a key role in granule morphology: higher amylose content tends to yield larger, often irregular granules. This structural variability can influence the physicochemical properties of starch, particularly its solubility, water-retention capacity, and behavior in solution.[61]

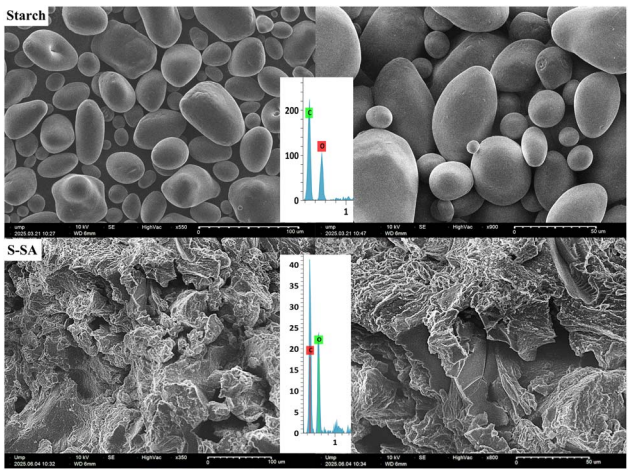

Fig. 12 SEM images and EDX spectra of starch and S-SA.

To examine the changes induced by the succinylation reaction, micrographs obtained by SEM were produced, as shown in Fig. 12. These images highlight clear morphological transformations between native starch and modified starch. Before modification, the starch surface had a smooth texture, with well-defined granules that were spherical to oval and relatively uniform in size. In contrast, after chemical modification, the granular structure becomes less apparent, replaced by an irregular surface marked by grooves, roughness, and partially porous areas. These alterations suggest a disruption of the starch's crystalline structure, probably due to the introduction of bulky succinate groups. In addition, the increase in porosity could be linked to partial swelling of the amorphous network, thus facilitating the accessibility of the reagents. The presence of these surface and internal transformations indirectly confirms the success of the chemical grafting and may also indicate a certain degree of cross-linking between the polysaccharide chains.[88] The EDX spectra in Fig. 12 clearly show the increase in the C/O ratio, with C/O = 2.003 for starch and C/O = 3.23 for S-MA; these values indicate an increase in carbon content in S-SA compared to starch, which can only be achieved by grafting succinate groups, indicating a good experimental approach for the esterification reaction.

3.4.4. X-ray diffraction patterns. Crystallinity is a key parameter in starch structural studies, encompassing both the assessment of relative crystallinity and the identification of crystalline polymorphs. This information is predominantly derived from XRD analyses.[89] In this study, the effect of starch dissolution in the DES composed of BTEAB/DMSO was investigated by examining changes in the crystalline structure and polymorphism of S-SA. XRD was employed to analyze alterations in the long-range crystalline order of both native and modified starch. The corresponding diffractograms are shown in Fig. 13a. Native starch exhibits several characteristic diffraction peaks at 2θ = 5.76°, 15.26°, 17.32°, 19.92°, 22.30°, 24.22°, 26.32°, 30.96°, and 34.4°, which are indicative of B-type crystallinity.[57] The crystallinity index (X_c) was calculated following the procedure outlined by L. S. Guinesi, *et al.*,[90] where H_c and H_a represent the intensities of the crystalline and amorphous peaks, respectively.

The crystallinity index of native starch reaches 80.75%. Amylose and amylopectin are the two main components of starch, with their contents being inversely proportional.[91] The crystallinity of starch granules is primarily influenced by the crystalline regions of amylopectin.[59] The S-SA exhibits a significantly reduced crystallinity compared to native starch, as evidenced by the disappearance of diffraction peaks at 2θ values of

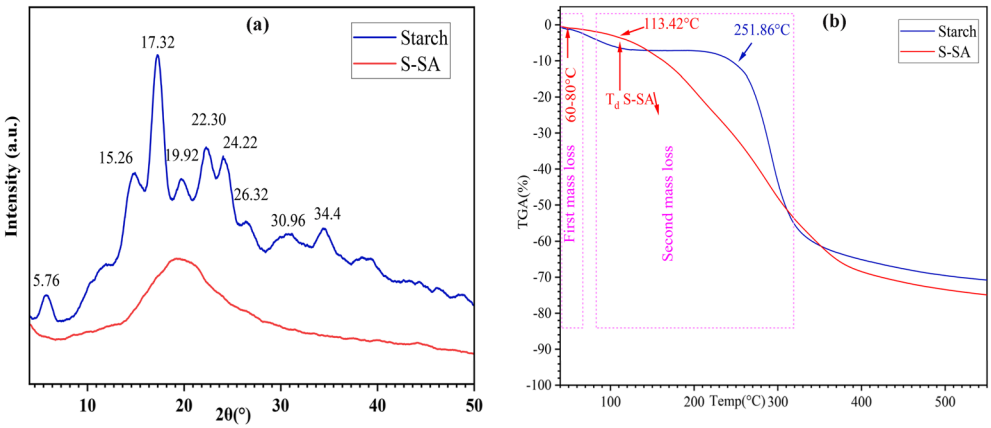

Fig. 13 (a) XRD spectra of SA and (b) TGA of starch and S-SA.

5.76°, 15.26°, 17.32°, 19.92°, 22.30°, 24.22°, 26.32°, 30.96°, and 34.4°, along with a pronounced broadening of the peak around 20.38°.[60] This structural modification leads to the emergence of a broad amorphous halo, reflecting a substantial loss of long-range crystalline order. The observed decrease in crystallinity is attributed to the disruptive effect of the BTEAB/DMSO-based DES, which effectively breaks down and disorganizes the native crystalline architecture of starch.

3.4.5. Thermal stability (TGA). Thermogravimetric analysis is used to assess the thermal stability and degradation behavior of organic materials. In this study, the thermal profiles of native starch and its esterified derivative, S-SA, were compared. The results reveal significant differences in the decomposition stages and degradation temperatures between the two samples. The TGA profiles indicate two major phases in the thermal degradation of starch. As shown in Fig. 13b, the TGA curve exhibits a marked change in degradation behavior between 200 °C and 400 °C. The shaded areas represent two separate stages of mass loss.[92] The first stage, observed at approximately 60–80 °C, corresponds to the indication of a single-step dehydration process.[92,93] After this stage, the sample remains thermally stable until reaching 251.86 °C. Above this threshold, a major degradation event occurs around 251.86 °C, suggesting single-step decomposition. This second stage represents the primary degradation phase of starch.[92] It is associated with the breakdown of both amorphous and crystalline domains.[33] At the final stage, when the temperature exceeds 500 °C, the material reaches thermal stability, resulting in the remaining mass being composed of mineral residue.[94]

The S-SA sample, with a degree of substitution of 0.82, exhibited a two-stage weight-loss profile. The initial weight loss at 60–80 °C was attributed to the endothermic evaporation of residual ethanol remaining from the precipitation and soxhlet extraction steps. This was followed by the thermal degradation of starch modified with succinic anhydride at 113.42 °C. Upon exceeding 500 °C, the material achieved thermal stability, leaving a residue corresponding to the mineral fraction of S-SA.[94] Similar results were reported by Fazal Haq *et al.*, where the decrease in starch crystallinity after esterification was explained by the introduction of succinyl groups that disrupted the regular organization of amylose and amylopectin chains. Replacing hydroxyl groups with ester groups weakened hydrogen bonding, leading to a more disordered, amorphous structure. This reduction in crystalline order resulted in lower thermal stability, as amorphous regions are more prone to thermal degradation. Moreover, succinyl ester linkages are less stable than glycosidic bonds, facilitating thermal cleavage at lower temperatures. Finally, the presence of carboxylic functions can catalyze degradation, explaining the decrease in the degradation temperature of S-SA.[95] The observed lower decomposition temperature for starch with a DS of 0.82 is likely a result of structural alterations within the starch granules caused by esterification. The diminished thermal stability of S-SA is probably due to a reduction in the number of hydroxyl groups within the starch structure, following ester formation. These observations are in agreement with earlier studies on anhydride-modified starches.[96,97] Similar findings were reported by Zhang *et al.*, who observed that the degradation onset temperature decreased from 277 °C for starch to 204 °C for the starch ester. This decrease in thermal stability is attributed to the introduction of carboxylic acid groups *via* esterification, which reduces the thermal stability of the starch-based resin.[98]

4 Conclusion

In this study, a new DES based on BTEAB and dimethyl sulfoxide (BTEAB/DMSO) was successfully prepared and reported for the first time. This innovative solvent system exhibited a remarkably low eutectic point of 0 °C. It demonstrated exceptional efficiency in dissolving starch, reaching solubility levels up to 22 wt%, far exceeding those typically achieved using conventional "green solvents". Beyond its dissolving capacity, the BTEAB/DMSO-based DES served as an effective reaction medium for the catalyst-free succinylation of starch, providing a simpler, cleaner, and more sustainable alternative to traditional synthetic routes. Comprehensive characterization by FTIR-ATR, XRD, SEM, EDX, and TGA confirmed profound structural and morphological transformations in starch following dissolution and esterification. These changes included a significant loss of crystallinity, disappearance of

granular morphology, alteration of thermal stability, and explicit incorporation of succinyl groups, all confirming the successful chemical modification of the polymer. The ability of this DES to combine high solvation power with reactivity under mild conditions highlights its dual functionality as both a solvent and a catalytic platform. Overall, this work introduces a highly promising DES with unique physicochemical properties and strong potential for broader applications in biomass valorization. The BTEAB/DMSO system stands out as a robust, versatile, and environmentally friendly medium capable of reshaping current strategies of polysaccharide processing and green chemical transformation. Future investigations will aim to extend the use of this DES to other biopolymers and deepen our understanding of its solvation mechanisms, paving the way toward new sustainable solutions in polymer chemistry and materials science.

Author contributions

Mohamed El Farkhani: writing-original draft, visualization, investigation, formal analysis, data curation. Omar Azougagh: writing-review & editing, validation. Mohamed Azzouzi: writing-review & editing. Said Dadou: writing-review & editing, validation. Meryem Abida: writing-review & editing, validation. Mohamed El Miz: writing-review & editing, resources. Soufian El Barkany: writing-review & editing, validation. Noureddine Benchat: writing-review & editing. Mohammed Koudad: visualization, validation, supervision, methodology, conceptualization.

Conflicts of interest

The authors state that there are no financial interests or personal relationships that might have affected the objectivity of the work described in this article.

Data availability

Data will be made available upon request.

Supplementary information (SI) is available. See DOI: https://doi.org/10.1039/d5ra08988c.

Acknowledgements

We sincerely thank the anonymous reviewers for their thorough evaluation and insightful remarks that helped improve this manuscript. The authors are also profoundly indebted to Professor Mohamed Abou-Salama, Director of the Laboratory of Molecular Chemistry, Materials and Environment (LCM2E) at the Faculty of Multidisciplinary Studies in Nador, for his unwavering support and fruitful collaboration. Our gratitude is also extended to Professor Abdelmonaem Talhaoui, Head of the Department of Physical Measurements at the Faculty of Sciences in Oujda, for providing essential facilities and financial assistance, which were crucial to the successful completion of this research.

References

1 M. J. Santander-Ortega, T. Stauner, B. Loretz, J. L. Ortega-Vinuesa, D. Bastos-González, G. Wenz, U. F. Schaefer and C. M. Lehr, *J. Controlled Release*, 2010, **141**, 85–92.
2 F. Zhu, *Carbohydr. Polym.*, 2015, **122**, 456–480.
3 K. Huber and J. BeMiller, *Carbohydr. Polym.*, 2000, **41**, 269–276.
4 S. Radosta, M. Haberer and W. Vorwerg, *Biomacromolecules*, 2001, **2**, 970–978.
5 W. Wang, H. Wang, X. Jin, H. Wang, T. Lin and Z. Zhu, *Polymer*, 2018, **153**, 643–652.
6 X. Lv, Y. Hong, Z. Gu, L. Cheng, Z. Li, C. Li and X. Ban, *Carbohydr. Polym.*, 2024, **329**, 121770.
7 A. C. Wu, E. Li and R. G. Gilbert, *Carbohydr. Polym.*, 2014, **114**, 36–42.
8 N. Koganti, J. R. Mitchell, R. N. Ibbett and T. J. Foster, *Biomacromolecules*, 2011, **12**, 2888–2893.
9 L. Zeng, W. Mao, J. Hao, G. Ye, X. Song, L. Zeng, S. Wang and J. Zhou, *Ind. Crops Prod.*, 2022, **177**, 114453.
10 C. Chi, Y. He, W. Jiao, H. Wang and X. Tan, *Ind. Crops Prod.*, 2022, **178**, 114672.
11 Z. He, M. W. Woo, Z. Shan, R. Dai, F. Cheng and H. Chen, *Colloids Surf., A*, 2022, **650**, 129544.
12 C. Cao, B. Nian, Y. Li, S. Wu and Y. Liu, *J. Agric. Food Chem.*, 2019, **67**, 12366–12373.
13 X. Tan, Y. Wang, W. Du and T. Mu, *ChemSusChem*, 2020, **13**, 321–327.
14 F. Ren, J. Wang, F. Xie, K. Zan, S. Wang and S. Wang, *Green Chem.*, 2020, **22**, 2162–2183.
15 A. P. Abbott, P. M. Cullis, M. J. Gibson, R. C. Harris and E. Raven, *Green Chem.*, 2007, **9**, 868–872.
16 D. Yu, Z. Xue and T. Mu, *Chem. Soc. Rev.*, 2021, **50**, 8596–8638.
17 E. L. Smith, A. P. Abbott and K. S. Ryder, *Chem. Rev.*, 2014, **114**, 11060–11082.
18 D. Yu, D. Jiang, Z. Xue and T. Mu, *Green Chem.*, 2024, **26**, 7478–7507.
19 D. Shi, F. Zhou, W. Mu, C. Ling, T. Mu, G. Yu and R. Li, *Phys. Chem. Chem. Phys.*, 2022, **24**, 26029–26036.
20 B. Zhang, F. Xie, J. L. Shamshina, R. D. Rogers, T. McNally, P. J. Halley, R. W. Truss, L. Chen and S. Zhao, *ACS Sustain. Chem. Eng.*, 2017, **5**, 3737–3741.
21 B. Soares, D. J. Tavares, J. L. Amaral, A. J. Silvestre, C. S. Freire and J. A. Coutinho, *ACS Sustain. Chem. Eng.*, 2017, **5**, 4056–4065.
22 O. Azougagh, I. Jilal, L. Jabir, H. El-Hammi, S. Essayeh, N. Mohammed, N. Achalhi, A. El Idrissi, Y. El Ouardi and K. Laatikainen, *Phys. Chem. Chem. Phys.*, 2023, **25**, 22870–22888.
23 Y. Chen and T. Mu, *Green Energy Environ.*, 2019, **4**, 95–115.
24 M. Zdanowicz and T. Spychaj, *Polimery*, 2011, **56**, 861–864.
25 H. B. Phan, C. M. Luong, T. H. Nguyen, L. D. Nguyen, K. N. Tran, H.-T. T. Nguyen and P. H. Tran, *Biomass Bioenergy*, 2023, **174**, 106855.
26 O. Azougagh, S. Essayeh, N. Achalhi, A. El Idrissi, H. Amhamdi, M. Loutou, Y. El Ouardi, A. Salhi, M. Abou-

Salama and S. El Barkany, *Carbohydr. Polym.*, 2022, **276**, 118737.
27 M. Elomaa, T. Asplund, P. Soininen, R. Laatikainen, S. Peltonen, S. Hyvärinen and A. Urtti, *Carbohydr. Polym.*, 2004, **57**, 261–267.
28 R. A. Alshaikh, E. A. Essa and G. M. El Maghraby, *Int. J. Pharm.*, 2019, **563**, 395–405.
29 M. M. Abdelquader, S. Li, G. P. Andrews and D. S. Jones, *Eur. J. Pharm. Biopharm.*, 2023, **186**, 85–104.
30 Y. Zhang, Y. Su and X. Ge, *J. China Univ. Sci. Technol.*, 1995, **25**, 474–478.
31 H. Ke, *Appl. Therm. Eng.*, 2017, **113**, 1319–1331.
32 I. Jilal, S. El Barkany, Z. Bahari, O. Sundman, A. El Idrissi, A. Salhi, M. Abou-Salama, M. Loutou and H. Amhamdi, *Cellulose*, 2018, **25**, 4375–4388.
33 H. El-Hammi, S. El Barkany, L. Jabir, O. Azougagh, I. Jilal, N. Achalhi, A. Salhi, A. El Idrissi, Y. El Ouardi and M. Abou-Salama, *Cellulose*, 2024, **31**, 2079–2103.
34 Y. Song, J. Zhang, W. Gan, J. Zhou and L. Zhang, *Ind. Eng. Chem. Res.*, 2010, **49**, 1242–1246.
35 D. E. Boldrini, *Carbohydr. Polym.*, 2025, 123249.
36 Y. Xu, V. Miladinov and M. A. Hanna, *Cereal Chem.*, 2004, **81**, 735–740.
37 C. I. K. Diop, H. L. Li, B. J. Xie and J. Shi, *Food Chem.*, 2011, **126**, 1662–1669.
38 S. Mathew and T. E. Abraham, *Food Chem.*, 2007, **105**, 579–589.
39 J. Fang, P. Fowler, J. Tomkinson and C. Hill, *Carbohydr. Polym.*, 2002, **47**, 245–252.
40 W. Ghezali, K. D. O. Vigier, R. Kessas and F. Jérôme, *Green Chem.*, 2015, **17**, 4459–4464.
41 A. P. Abbott, G. Capper, D. L. Davies, R. K. Rasheed and V. Tambyrajah, *Chem. Commun.*, 2003, 70–71.
42 Q. Zhang, K. D. O. Vigier, S. Royer and F. Jérôme, *Chem. Soc. Rev.*, 2012, **41**, 7108–7146.
43 A. Biswas, R. Shogren, D. Stevenson, J. Willett and P. K. Bhowmik, *Carbohydr. Polym.*, 2006, **66**, 546–550.
44 M. Zdanowicz, *Carbohydr. Polym.*, 2020, **229**, 115574.
45 O. Azougagh, I. Jilal, L. Jabir, H. El-Hammi, S. Essayeh, N. Mohammed, N. Achalhi, R. El yousfi, A. El Idrissi, Y. El Ouardi, K. Laatikainen, M. Abou-Salama and S. El Barkany, *Phys. Chem. Chem. Phys.*, 2023, **25**, 22870–22888.
46 F. Puspasari, B. Airlangga, P. N. Trisanti and Sumarno, *IOP Conf. Ser.:Mater. Sci. Eng.*, 2019, **673**, 012135.
47 L. Boetje, X. Lan, F. Silvianti, J. van Dijken, M. Polhuis and K. Loos, *Carbohydr. Polym.*, 2022, **292**, 119649.
48 H. Winkler, W. Vorwerg and H. Wetzel, *Carbohydr. Polym.*, 2013, **98**, 208–216.
49 X. Xiao, Y. Sun, J. Liu and H. Zheng, *Sep. Purif. Technol.*, 2021, **267**, 118628.
50 J. F. Mano, D. Koniarova and R. Reis, *J. Mater. Sci.:Mater. Med.*, 2003, **14**, 127–135.
51 V. P. Cyras, M. C. Tolosa Zenklusen and A. Vázquez, *J. Appl. Polym. Sci.*, 2006, **101**, 4313–4319.
52 R. Kizil, J. Irudayaraj and K. Seetharaman, *J. Agric. Food Chem.*, 2002, **50**, 3912–3918.
53 J. J. Cael, J. L. Koenig and J. Blackwell, *Biopolym. Original Res. Biomol.*, 1975, **14**, 1885–1903.
54 M. Miao, R. Li, B. Jiang, S. W. Cui, T. Zhang and Z. Jin, *Food Chem.*, 2014, **151**, 154–160.
55 T. Yoshimura, R. Yoshimura, C. Seki and R. Fujioka, *Carbohydr. Polym.*, 2006, **64**, 345–349.
56 W.-f. Han, Q.-l. Lin, S.-m. Zhao, J.-t. Li and G.-h. Niu, *Shipin Kexue/Food Sci.*, 2020, **41**, 267–275.
57 C. Pozo, S. Rodríguez-Llamazares, R. Bouza, L. Barral, J. Castaño, N. Müller and I. Restrepo, *J. Polym. Res.*, 2018, **25**, 1–8.
58 N. W. H. Cheetham and L. Tao, *Carbohydr. Polym.*, 1997, **33**, 251–261.
59 J. J. Van Soest and J. F. Vliegenthart, *Trends Biotechnol.*, 1997, **15**, 208–213.
60 N. A. Abd El-Ghany and Z. M. Mahmoud, *Polym. Bull.*, 2021, **78**, 6161–6182.
61 P. A. Méndez, Á. M. Méndez, L. N. Martínez, B. Vargas and B. L. López, *Int. J. Biol. Macromol.*, 2022, **205**, 1–14.
62 M. Sujka and J. Jamroz, *Food Hydrocolloids*, 2013, **31**, 413–419.
63 W. Rahman, L. T. Sin, A. Rahmat and A. Samad, *Carbohydr. Polym.*, 2010, **81**, 805–810.
64 D. Shen and S. Gu, *Bioresour. Technol.*, 2009, **100**, 6496–6504.
65 D. A. Fort, R. C. Remsing, R. P. Swatloski, P. Moyna, G. Moyna and R. D. Rogers, *Green Chem.*, 2007, **9**, 63–69.
66 A. S. Amarasekara, Y. M. Lawrence, V. C. Nwankwo and N. Shamim, *Polym. Sci., Ser. A*, 2023, **65**, 53–62.
67 S. Ptak, A. Zarski and J. Kapusniak, *Materials*, 2020, **13**, 4479.
68 F. Haq, H. Yu, Y. Wang, L. Wang, S. Mehmood, M. Haroon, S. Fahad, M. A. Uddin and D. Shen, *J. Polym. Environ.*, 2021, **29**, 2676–2685.
69 F. Cao, S. Lu and S. Y. Quek, *Int. J. Biol. Macromol.*, 2023, **253**, 126579.
70 S. Sun, X. Lin, B. Zhao, B. Wang and Z. Guo, *Lwt*, 2020, **117**, 108698.
71 J. Zhou, L. Ren, J. Tong, L. Xie and Z. Liu, *Carbohydr. Polym.*, 2009, **78**, 888–893.
72 Y. Zuo, J. Gu, L. Yang, Z. Qiao, H. Tan and Y. Zhang, *Int. J. Biol. Macromol.*, 2013, **62**, 241–247.
73 M. J. Tizzotti, M. C. Sweedman, D. Tang, C. Schaefer and R. G. Gilbert, *J. Agric. Food Chem.*, 2011, **59**, 6913–6919.
74 Z. Xiong, S. Ma, L. Fan, Z. Tang, R. Zhang, H. Na and J. Zhu, *Compos. Sci. Technol.*, 2014, **94**, 16–22.
75 P. Caputo, V. Loise, M. F. Colella, M. Porto, R. A. Salvino, C. O. Rossi and G. De Luca, *Phys. Chem. Chem. Phys.*, 2023, **25**, 26014–26022.
76 Y. Hao, Y. Chen, Q. Li and Q. Gao, *Ind. Crops Prod.*, 2019, **130**, 111–117.
77 S. R. Goswami, S. Wang, P. Gnanasekar, P. Chauhan and N. Yan, *Carbohydr. Polym.*, 2020, **234**, 115892.
78 R. Rohan, T.-C. Kuo, C.-Y. Chiou, Y.-L. Chang, C.-C. Li and J.-T. Lee, *J. Power Sources*, 2018, **396**, 459–466.
79 H. Liu, L. Yu, G. Simon, X. Zhang, K. Dean and L. Chen, *Carbohydr. Res.*, 2009, **344**, 350–354.
80 Z. Qiao, J. Gu, S. Lv, J. Cao, H. Tan and Y. Zhang, *BioResources*, 2016, 11.

81 N. Supanchaiyamat, *Bio-based thermoset composites from epoxidised linseed oil*, University of York, 2012.
82 L. Tang, B. Huang, N. Yang, T. Li, Q. Lu, W. Lin and X. Chen, *Green Chem.*, 2013, **15**, 2369–2373.
83 F. Zhu, *Food Hydrocolloids*, 2017, **63**, 611–624.
84 H. Liu, L. Yu, G. Simon, X. Zhang, K. Dean and L. Chen, *Carbohydr. Res.*, 2009, **344**, 350–354.
85 H. Pan, T. F. Shupe and C. Y. Hse, *J. Appl. Polym. Sci.*, 2008, **108**, 1837–1844.
86 N. Achalhi, Y. El Ouardi, R. El Yousfi, A. Abarkan, S. El Barkany and A. El Idrissi, *Int. J. Biol. Macromol.*, 2025, **311**, 143968.
87 Y. Liu, H. Xie and M. Shi, *Starch Staerke*, 2016, **68**, 683–690.
88 M. D. Teli and A. Mallick, *J. Polym. Environ.*, 2018, **26**, 1581–1591.
89 A. Lopez-Rubio, B. Flanagan, E. Gilbert and M. Gidley, *Biopolymers*, 2008, **89**, 761–768.
90 L. S. Guinesi, A. L. da Róz, E. Corradini, L. H. C. Mattoso, E. d. M. Teixeira and A. A. d. S. Curvelo, *Thermochim. Acta*, 2006, **447**, 190–196.
91 N. Cheetam and L. Tao, *Carbohydr. Res.*, 1997, **33**, 251–261.
92 B. Janković, *Carbohydr. Polym.*, 2013, **95**, 621–629.
93 X. Wang, L. Cheng, Z. Li, C. Li, X. Ban, Z. Gu and Y. Hong, *Int. J. Biol. Macromol.*, 2022, **223**, 1684–1692.
94 M. C. Posada-Velez, P. Pineda-Gomez and H. D. Martinez-Hernandez, *Environ. Nanotechnol. Monit. Manag.*, 2023, **20**, 100786.
95 F. Haq, H. Yu, Y. Wang, L. Wang, S. Mehmood, M. Haroon, A. Bilal Ul, S. Fahad, M. A. Uddin and D. Shen, *J. Polym. Environ.*, 2021, **29**, 2676–2685.
96 L. Zhang, W. Xie, X. Zhao, Y. Liu and W. Gao, *Thermochim. Acta*, 2009, **495**, 57–62.
97 P. Cuenca, S. Ferrero and O. Albani, *Food Hydrocolloids*, 2020, **100**, 105430.
98 S.-D. Zhang, Y.-R. Zhang, H.-X. Huang, B.-Y. Yan, X. Zhang and Y. Tang, *J. Polym. Res.*, 2010, **17**, 43–51.